Caspase-8 induces cleavage of gasdermin D to elicit pyroptosis during *Yersinia* infection

Joseph Sarhan[a,b,c,1], Beiyun C. Liu[a,c,1], Hayley I. Muendlein[c,d], Peng Li[e], Rachael Nilson[c], Amy Y. Tang[c], Anthony Rongvaux[f], Stephen C. Bunnell[c], Feng Shao[e], Douglas R. Green[g], and Alexander Poltorak[c,h,2]

[a]Graduate Program in Immunology, Tufts University Sackler School of Biomedical Sciences, Boston, MA 02111; [b]Medical Scientist Training Program, Tufts University School of Medicine, Boston, MA 02111; [c]Department of Immunology, Tufts University School of Medicine, Boston, MA 02111; [d]Graduate Program in Genetics, Tufts University Sackler School of Biomedical Sciences, Boston, MA 02111; [e]Collaborative Innovation Center for Cancer Medicine, National Institute of Biological Sciences, 102206 Beijing, China; [f]Program in Immunology, Clinical Research Division, Fred Hutchinson Cancer Research Center, Seattle, WA 98109; [g]Department of Immunology, St. Jude Children's Research Hospital, Memphis, TN 38104; and [h]Center of High Biomedical Technologies, Petrozavodsk State University, Petrozavodsk, Republic of Karelia, 185910, Russia

Edited by Eicke Latz, University of Bonn, Bonn, Germany, and accepted by Editorial Board Member Peter Palese October 7, 2018 (received for review June 5, 2018)

Cell death and inflammation are intimately linked during *Yersinia* infection. Pathogenic *Yersinia* inhibits the MAP kinase TGFβ-activated kinase 1 (TAK1) via the effector YopJ, thereby silencing cytokine expression while activating caspase-8–mediated cell death. Here, using *Yersinia pseudotuberculosis* in corroboration with costimulation of lipopolysaccharide and (5Z)-7-Oxozeaenol, a small-molecule inhibitor of TAK1, we show that caspase-8 activation during TAK1 inhibition results in cleavage of both gasdermin D (GSDMD) and gasdermin E (GSDME) in murine macrophages, resulting in pyroptosis. Loss of GsdmD delays membrane rupture, reverting the cell-death morphology to apoptosis. We found that the *Yersinia*-driven IL-1 response arises from asynchrony of macrophage death during bulk infections in which two cellular populations are required to provide signal 1 and signal 2 for IL-1α/β release. Furthermore, we found that human macrophages are resistant to YopJ-mediated pyroptosis, with dampened IL-1β production. Our results uncover a form of caspase-8–mediated pyroptosis and suggest a hypothesis for the increased sensitivity of humans to *Yersinia* infection compared with the rodent reservoir.

pyroptosis | caspase-8 | gasdermin | *Yersinia* | TAK1

Cell death and inflammation are critical regulators of immune responses which must be carefully balanced to ensure host survival during infection. Upon initial pathogen contact with innate immune cells, the host cell signaling through Toll-like receptors (TLRs) simultaneously engages a cell's intrinsic prosurvival program and produces inflammatory cytokines to propagate the alarm of infection (1). These cytokines are critical for the activation and recruitment of further waves of innate and adaptive immunity as well as for reinforcing the inflammation loop via autocrine signaling in the current population. Successful pathogens have therefore evolved ways to evade host cytokine induction to survive and replicate silently among host immune cells. This is done either by modifying surface pathogen-associated molecular patterns that cannot be recognized by macrophage TLRs or via active blockade of macrophage-signaling pathways downstream of TLR activation (2).

To counteract the latter, these same prosurvival, procytokine signaling pathways also have built-in switches to engage cell death when the cell perceives a block to its ability to produce cytokines (3). One of the best-characterized examples of such a switch lies downstream of TNF receptor. TNF receptor signaling engages the TNF receptor-associated adaptor TRADD to recruit RIP1 via death domain (DD) interactions (4), forming complex I. Complex I formation results in the activation of the MAP kinases and NFκB, which drive the production of inflammatory cytokines and prosurvival factors (5). When MAP kinases and/or NFκB signaling are blocked, RIP1 dissociates from TNF receptor to facilitate the formation of complex IIa by interacting with FADD and pro–caspase-8. Complex IIa leads to caspase-8 activation and cell death (6). If caspase activity is blocked, the signaling complex transitions to complex IIb, in which RIP1 engages RIP3 to activate an MLKL-dependent necrotic cell-death mechanism known as "necroptosis" (7). In recent years necroptosis has similarly been shown to occur downstream of TLR signaling (8).

The success of MAP kinase and NFκB signaling thus are critical determinants of the life and death of a cell. MAP kinase and NFκB pathways diverge from a single protein complex consisting of TGFβ-associated kinase (TAK1), TAB1, and TAB2 in which TAK1 experiences constitutive phosphorylation and baseline activity (9). In mice, whole-body TAK1 deficiency results in lethality between E9.5–E10.5 (10). Follow-up studies elucidated that TNF stimulation in the context of TAK1 deficiency leads to cell death via caspases (complex IIa) or, in the case of caspase inhibition, to cell death by necroptosis (complex IIb) (11, 12). Similarly, whole-body RIP1 deficiency results in perinatal lethality in which *Rip1*$^{-/-}$ and conditionally null animals show exquisite sensitivity to tonic TNF-induced cell death (5, 13).

Given the intertwining relationship between cytokine production and cell death during infection, the central question thus becomes what is achieved upon cell death if cytokines, the universal alarms, cannot be adequately made in the first place. The well-studied bacteria of the *Yersinia* species may lend an answer.

Significance

Here we demonstrate that *Yersinia* YopJ-induced murine macrophage death involves caspase-8–induced cleavage of both gasdermin D (GSDMD) and gasdermin E (GSDME). The ensuing cell death is rapid, morphologically is similar to pyroptosis, and induces IL-1 release. Recently, both GSDMD and GSDME were reported to be critical effectors of caspase-1/11–driven pyroptosis and caspase-3–dependent secondary necrosis, which prompted the redefinition of pyroptosis as cell death-mediated by gasdermin activation. Our work extends these studies and shows that activation of caspase-8 in the context of TAK1 inhibition results in cleavage of both GSDMD and GSDME, leading to pyroptotic-like cell death. Further study will be needed to determine whether caspase-8 cleaves GSDMD directly or via intermediate substrates.

Author contributions: J.S. and B.C.L. designed research; J.S., B.C.L., H.I.M., P.L., R.N., and A.Y.T. performed research; A.R. and F.S. contributed new reagents/analytic tools; J.S., B.C.L., S.C.B., and D.R.G. analyzed data; and J.S., B.C.L., and A.P. wrote the paper.

The authors declare no conflict of interest.

This article is a PNAS Direct Submission. E.L. is a guest editor invited by the Editorial Board.

[1]J.S. and B.C.L. contributed equally to this work.

[2]To whom correspondence should be addressed. Email: Alexander.Poltorak@tufts.edu.

This article contains supporting information online at www.pnas.org/lookup/suppl/doi:10.1073/pnas.1809548115/-/DCSupplemental.

Published online October 31, 2018.

Yersinia species express a number of *Yersinia* outer proteins (Yops) that manipulate various macrophage cytosolic processes (14). One such protein, YopJ, inhibits TAK1 via acetylation (15) with consequent induction of macrophage cell death (16). *Yersinia*-induced cell death was recently shown to be caspase-8 dependent but RIP3 independent. Paradoxically, while *Rip3*$^{-/-}$*Casp8*$^{-/-}$ macrophages are protected from cell death, the animals succumb to the infection, with higher bacterial burden in various solid organs (17). Similarly, *Yersinia*-induced macrophage cell death is strongly dependent on RIP1 kinase activity; RIP1 kinase-inactive animals also show increased sensitivity to infection (18). These studies suggest that macrophage death in the context of *Yersinia* infection is protective for the animal host.

Interestingly, despite the ability of YopJ to dampen cytokine production, *Yersinia* infections in mice elicit a robust IL-1 response, with IL-1 receptor signaling playing a crucial role in the survival of the animal (19). IL-1 maturation requires the formation of a caspase nucleation event termed the "inflammasome." The inflammasome is triggered via the sensing of a cytosolic "danger" signal that nucleates multiple units of procaspase-1 for proximity-induced autocleavage and activation. One of the best-studied inflammasomes is the NLRP3 inflammasome, which nucleates in response to bacterial components, crystals, or potassium efflux. NLRP3 recruits apoptosis-associated speck-like protein (ASC), which then recruits procaspase-1 via homotypic CARD-domain binding (20). Caspase-1 is activated via autocleavage by which active caspase-1 cleaves pro–IL-1β and pro–IL-18. The release of mature IL-1β in conjunction with inflammasome-driven cell death is termed "pyroptosis" (11). With the discovery that caspase-11 drives pyroptosis via activation of the pore-forming protein gasdermin D (GSDMD) (12), the NLRP3 inflammasome was found to activate as a consequence of plasma membrane rupture and the concurrent efflux of potassium ions (21). More recently, activation of the NLRP3 inflammasome has also been observed during necroptosis (22), suggesting that inflammasome formation may be a commonality shared among many necrotic forms of cell death.

In this work, we set out to investigate the morphological features of the caspase-8–driven cell death during TAK1 inhibition, using *Yersinia pseudotuberculosis* as our infection model. To model a complex infection system to minimal manipulable units, we additionally use LPS and 5Z-7-Oxozeaenol (5z7), a potent small-molecule inhibitor of TAK1 (23), to mimic the basic cell-death phenotype induced by *Yersinia*. We found that *Yersinia*-induced cell death bears a striking morphologic resemblance to pyroptosis, the involvement of multiple gasdermins, and the potency of IL-1 production. This led us to conclude that caspase-8 can drive pyroptosis in cases of TAK1 inhibition during inflammatory signaling.

Results

During TAK1 Inhibition, TLR Stimulation Drives Caspase-8–Dependent Cell Death with Necroptosis as a Backup Mechanism. *Yersinia* species, including *Yersinia pestis* and *Y. pseudotuberculosis*, induce macrophage cell death via effector YopJ inhibition of the level-three MAP kinase TAK1 (15). We used nuclear incorporation of propidium iodide (PI) to monitor the kinetics of cell membrane integrity loss in real time. We see that in B6 macrophages YopJ-specific macrophage death occurs is complete by 4–6 h post bacterial challenge and that macrophages lacking both RIP3 and caspase-8 are protected (*SI Appendix*, Fig. S1.1*A*), consistent with published reports (17). To investigate the individual contribution of caspase-8 and RIP3, we used the small-molecule inhibitors zVAD for pan-caspase inhibition or Nec1 for inhibition of necroptotic machinery. We find that *Y. pseudotuberculosis*-driven cell death can be partially rescued by inhibition of caspases or RIP kinases; however, complete ablation of *Yersinia*-driven cell death requires the addition of both zVAD and Nec1 (Fig. 1*A*, *Left*). We can effectively mimic this response by costimulation of macrophages with the small-molecule inhibitor of TAK1 5z7 in combination with a TLR agonist, in this case LPS (Fig. 1*A*, *Right* and *SI Appendix*, Fig. S1.1*B*).

Necrostatin-1 (Nec1), the small-molecule inhibitor of RIP1 kinase activity, is used to block necroptosis driven by RIP1/RIP3 and the effector of necroptotic cell death, MLKL (24). Given the partial protection with Nec1, we investigated the contribution of necroptotic players during *Yersinia*-driven as well as LPS/5z7-driven cell death. Using genetic knockouts of RIP3 and MLKL, we found that *Mlkl*$^{-/-}$ and *Rip3*$^{-/-}$ macrophages are fully susceptible to *Yersinia*- and LPS/5z7-driven cell death (Fig. 1*B* and *SI Appendix*, Fig. S1.1*C*). With the addition of zVAD, *Rip3*$^{-/-}$ and *Mlkl*$^{-/-}$ macrophages become protected from death, indicating that in the context of TAK1 inhibition necroptosis is engaged only when caspase activity is blocked. However, the full susceptibility of RIP3- and MLKL-deficient cells to *Yersinia*-driven death argues that necroptosis is not the primary pathway of cell death during *Yersinia* infection. The addition of Nec1 during *Yersinia* challenge or LPS/5z7 stimulation shows partial protection regardless of the presence of RIP3 or MLKL.

Working upstream in the pathway, RIP1 kinase activity plays critical roles for the initiation of necroptosis during caspase inhibition (25). However, RIP1 also has a role in TNF-driven apoptosis via the formation of complex II (6). We found that RIP1 kinase-inactive (RIP1$^{K45A/K45A}$) macrophages are partially protected from *Yersinia*- and LPS/5z7-driven cell death, recapitulating the effect of Nec1 addition (Fig. 1*C*) (18). RIP3 kinase-inactive (RIP3$^{K51A/K51A}$) macrophages behave like *Rip3*$^{-/-}$ macrophages (*SI Appendix*, Fig. S1.1*D*), and RIP1/3 double-kinase–inactive macrophages show susceptibility similar to that of RIP1 single-kinase macrophages (Fig. 1*C* and *SI Appendix*, Fig. S1.1*E*). RIP1 thus plays an enhancement role in driving cell death during *Yersinia* infection but is not the critical factor. Confirming previous findings (17), cells deficient for both RIP3 and caspase-8 are fully protected from *Yersinia*- and LPS/5z7-driven cell death (Fig. 1*D*). We expand on this finding and show that macrophages lacking RIP3 and FADD are equally resistant to *Yersinia*-induced and LPS/5z7-induced cell death (Fig. 1*E*). Given that *Rip3*$^{-/-}$ macrophages are fully sensitive to cell death, the full protection provided by the additional loss of caspase-8 or FADD indicates that caspase-8/FADD complex is necessary to drive cell death. *Yersinia* as well as TLR stimulation under TAK1 inhibition thus drives a mode of rapid, cell death that is caspase-8 driven, with a partial contribution from RIP kinase 1.

TAK1 kinase activity is critical for the activation of the MAP kinase- and NFκB-signaling pathways. To address the individual roles of MAP kinases and NFκB in TAK1-induced cell death, we stimulated B6 macrophages with LPS in the presence of various MAPK and IKKβ inhibitors. Treatment of LPS-stimulated cells with p38, JNK, or MEK1/2 inhibitors individually was not sufficient to induce cell death to the extent observed in cells stimulated with LPS + 5z7 (*SI Appendix*, Fig. S1.2*A*). However, treatment of LPS-stimulated cells with a combination of p38 and JNK inhibitors resulted in cell death more potently than induced by either inhibitor independently (*SI Appendix*, Fig. S1.2*A*). Treatment of LPS-stimulated macrophages with various IKKβ inhibitors induces cell death in a manner similar to TAK1 inhibition (*SI Appendix*, Fig. S1.2*B*). Both MAPK inhibition- and NFκB inhibition-dependent cell death are similarly absent in *RIP3*$^{-/-}$*Casp8*$^{-/-}$ macrophages (*SI Appendix*, Fig. S1.2 *A* and *B*).

Using TLR adaptor-deficient bone marrow-derived macrophages (BMDMs), we found that LPS + 5z7-induced cell death can occur independently of the TLR4 adaptor MyD88 and is fully sufficient in the setting of adequate TRIF signaling (*SI Appendix*, Fig. S1.3*A*). Interestingly, in the case of TRIF, LPS + 5z7 deficiency still induced cell death via MyD88 signaling, but the character of this cell death is different. The percentage of cell death is lower in TRIF deficiency, and, interestingly, the cell death is entirely dependent on RIPK activity, given its reversibility with Nec-1. To explore further the role of other TLR

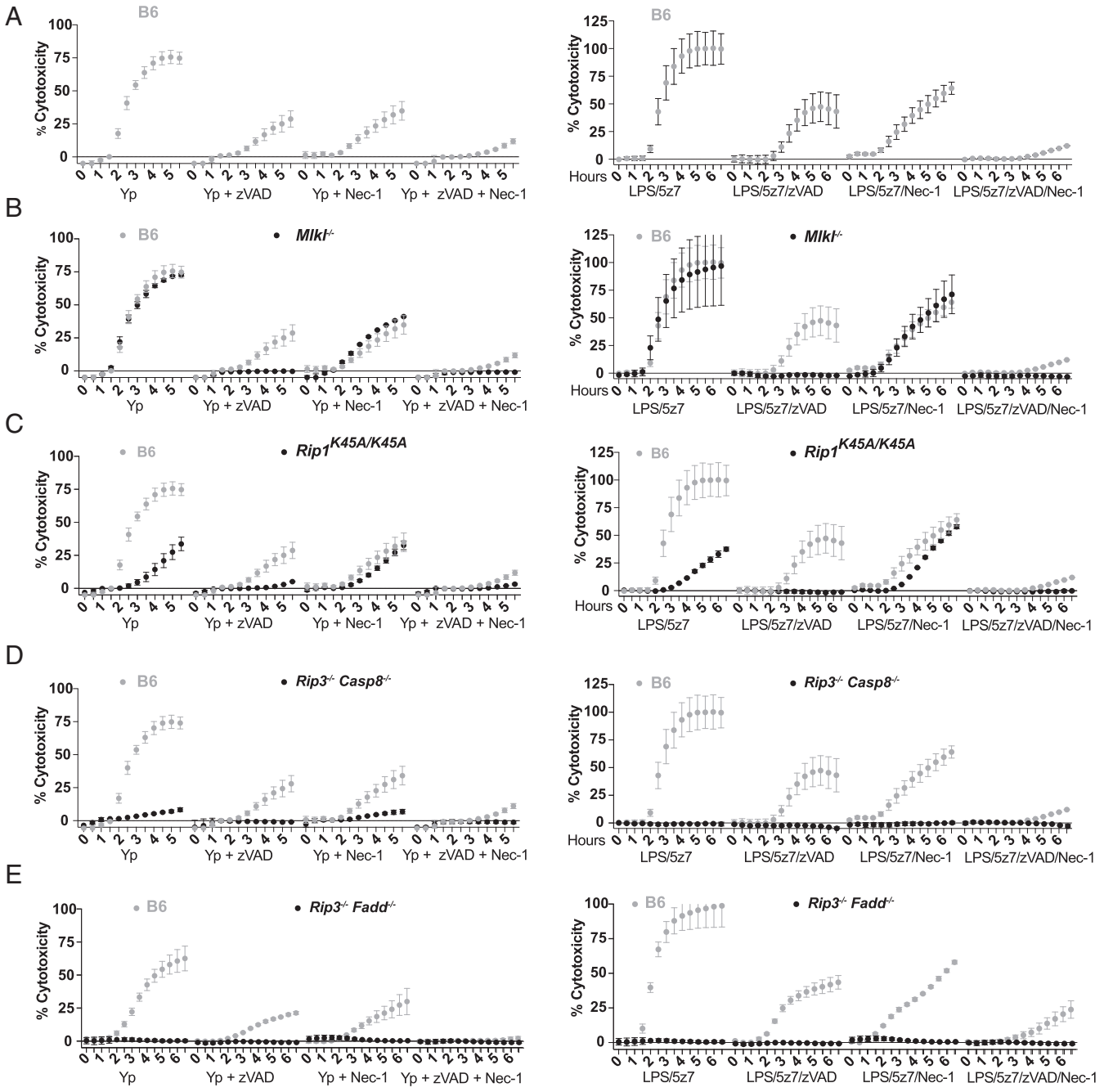

Fig. 1. During TAK1 inhibition, TLR stimulation drives caspase-8–dependent cell death, with necroptosis as a backup mechanism. BMDMs from C57BL/6 (B6) and various genetically modified animals were stimulated with *Y. pseudotuberculosis* IP2666 (*Left*) or LPS (10 ng/mL)/5z7 (125 nM) (*Right*). *Y. pseudotuberculosis* was infected at an MOI of 30. Percentage cytotoxicity was calculated by 4× microscopy via counting PI^+ nuclei per field of view, normalized to 100% lysis by 0.1% Triton X-100. Caspases were inhibited with zVAD treatment (50 μM), and RIP kinase activity was inhibited with Nec1 (10 μM). All inhibitors were added simultaneously at time 0. The cytotoxicity curve of each genotype is superimposed over B6 cytotoxicity curves (gray) for clarity of comparison. Data in *A–D* are from one experiment utilizing the same set of B6 controls; data in *E* are from an independent experiment. All kinetic cytotoxicity data are representative of at least three independent experiments. See related *SI Appendix*, Fig. S1.

adaptors, we stimulated B6 BMDMs stimulated with various TLR agonists or an SMAC mimetic in combination with 5z7 (*SI Appendix*, Fig. S1.3*B*) and observed faster kinetics of cell death with TLR stimulation or SMAC mimetic treatment than with 5z7 alone. Interestingly, LPS is unique in that it induces cell death in a TNF-independent manner (*SI Appendix*, Fig. S1.3*B*), whereas cell death induced by other TLR agonists + 5z7, SMAC mimetic + 5z7, or 5z7 alone is strongly TNF dependent. Interestingly, these TNF-dependent forms of cell death are also strongly dependent on RIP kinase activity, as indicated by the elimination of cell death with the addition of Nec-1. Much like type-I IFN, TNF is produced in resting cells (26, 27). The phenomenon of tonic TNF production likely underlies the basis of cell death in the setting of cell death induced by 5z7 alone.

TAK1 Inhibition Results in Externalization of Cytosolic Content with Pan-Caspase Cleavage. Traditionally, caspase-8 activation has been associated with apoptosis, characterized morphologically by

the shedding of apoptotic bodies and the retention of membrane integrity during cell death to promote efferocytosis over secondary necrosis and the release of cytosolic contents (28). However, the rapidity of PI uptake during *Yersinia*- and LPS/5z7-driven cell death is suggestive of necrotic cell death. Indeed, LPS/5z7 induces rapid and indiscriminate release of cytosolic contents into the surrounding culture medium as compared with the canonical apoptosis stimulant etoposide and the recently synthesized small-molecule raptinal, which drives cell death via caspase-9 activation of caspase-3 and -7 (Fig. 2*A*) (29).

Probing for caspase activation and their appearance in the culture medium (precipitated supernatant), we found that the majority of fragments corresponding to active caspase-8, caspase-9, caspase-3, and caspase-7 have accumulated extracellularly by 5 h of LPS/5z7 stimulation (Fig. 2*B*). In contrast, these cleaved caspase fragments can be seen by 5 h in cell lysates of etoposide-treated cells, but cleaved caspase-3 and caspase-7 are not seen in the supernatant until more than 16 h after stimulation.

Additional cytosolic contents released upon LPS/5z7 stimulation include cleaved poly (ADP-ribose) polymerase (PARP), cyclophilin A, and GAPDH. Congruent with the cell-death kinetics, the apoptosis machinery is blocked with addition of zVAD, which switches the cell fate to necroptosis, as indicated by the appearance of phosphorylated MLKL with zVAD addition (Fig. 2*C*). Using macrophages deficient for both RIP3 and caspase-8, we confirmed that the release of cytosolic content during LPS/5z7 stimulation occurs as a consequence of cell death. With *Rip3*$^{-/-}$ *Casp8*$^{-/-}$ macrophages, the cleavage of caspase-3 and PARP is no longer present beyond baseline levels, and cytosolic proteins such as cyclophilin A, GAPDH, and actin remain intracellular during LPS/5z7 stimulation (Fig. 2*D*).

We confirmed that 5z7 can inhibit both MAPK and NFκB signaling in the context of LPS signaling in BMDMs (*SI Appendix*, Fig. S2*A*). To rule out the contribution of cell death and to study the effects of the *Yersinia* effect on YopJ, we infected *RIP3*$^{-/-}$*Casp8*$^{-/-}$ macrophages with wild-type and YopJ-deficient (ΔJ) *Yersinia*. As early as 30 min after infection, wild-type *Yersinia* inhibits MAP kinase activation as measured by p38 and ERK (MEK1/2) phosphorylation. In contrast, the effect of YopJ on NFκB activation as measured by IKKα/β and p65 phosphorylation was attenuated (*SI Appendix*, Fig. S2*B*). In addition, the degradation and replenishment of the NFκB inhibitor IκB-α had similar kinetics in cells infected with wild-type *Yersinia* infection and cells infected with ΔJ *Yersinia* (*SI Appendix*, Fig. S2*B*). Collectively, these data agree with the previous reports that YopJ preferentially blocks the activation of MAPKs rather than of NFκB (30, 31).

***Yersinia*- and LPS/5z7-Driven Cell Death Resembles Pyroptosis by Morphology.** Apoptosis, necroptosis, and pyroptosis are morphologically distinct from each other. Using time-lapse microscopy, we followed the progression of macrophages undergoing each of these three well-defined modes of cell death to determine the morphology taken by cells dying from LPS/5z7 or *Yersinia* (Fig. 3 *A*–*E*).

For a rapid form of apoptosis, we use the small molecule raptinal, which engages caspase-9 activation (32). Raptinal-treated cells progress to membrane rupture by 2–3 h post stimulation, thus placing it on a timescale similar to LPS/5z7-induced cell death (Fig. 3*A*). Cells undergoing raptinal treatment display typical signs of cell shrinkage and extensive blebbing as early as 30 min post stimulation. Annexin V positivity as an indication of phosphatidylserine externalization is rampant by 40 min, and this phase is extended for at least 1 h. Two hours post stimulation the cell membrane ruptures as indicated by nuclear PI signal, with morphology of the dying cell marked by multiple necrotic bubbles resembling that of secondary necrosis (33).

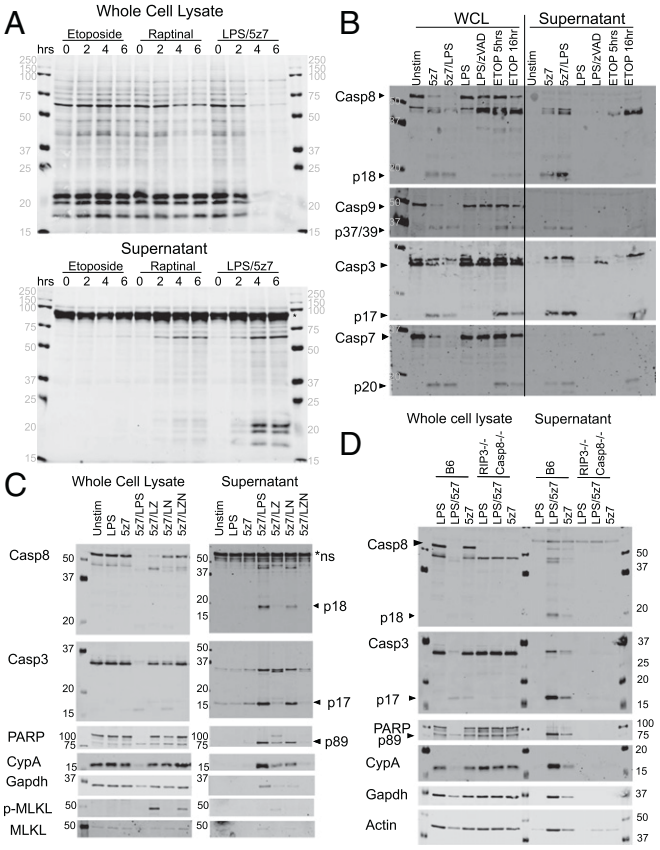

Fig. 2. TAK1 inhibition results in necrotic cell death, exhibiting pan-caspase activation and the externalization of cytosolic content. (*A*) BMDMs were stimulated with etoposide (150 μM), raptinal (10 μM), or LPS (10 ng/mL)/5z7 (125 nM) for 0–6 h. Cellular lysates (*Upper*) and precipitated supernatant (*Lower*) were run on SDS/PAGE gels, and total protein was stained by LiCOR total protein stain. The asterisk indicates serum proteins from residual FBS in the culture medium. (*B*) BMDMs were stimulated as indicated for 5 h, except for etoposide, which was stimulated for an additional 16 h. Cellular lysate and precipitated supernatant were run on SDS/PAGE gels and were probed for pro- and cleaved forms of various apoptotic caspases. (*C*) BMDMs were stimulated with LPS/5z7 for 5 h in the presence of zVAD (50 μM) or Nec1 (10 μM) to block caspase or RIP kinase activity, respectively. Cellular lysate and precipitated supernatant were run on SDS/PAGE gels and probed for caspases, the caspase substrate PARP, cytosolic proteins cyclophilin A (CypA), Gapdh, phosphorylated (S345) MLKL (p-MLKL), and total MLKL. (*D*) BMDMs from B6 and *Rip3*$^{-/-}$ *Casp8*$^{-/-}$ animals were stimulated with LPS, LPS/5z7, or 5z7 for 5 h. Cellular lysate and precipitated supernatant were run on SDS/PAGE gels and probed for caspases, the caspase substrate PARP, cytosolic proteins cyclophilin A (CypA), Gapdh, and actin. All Western blots are representative of three or more experiments.

Recently, Gong et al. (34) showed that necroptosis, although a necrotic form of cell death, can display phosphatidylserine externalization before membrane rupture. We confirm that with LPS/zVAD-induced necroptosis annexin V binding is evident by 50–60 min post stimulation in the absence of cell shrinkage as seen in apoptosis. Membrane ruffling is seen during the annexin V-positive phase, and plasma membrane rupture takes the form of one or two large necrotic bubbles per cell that coincides with nuclear PI positivity. Necroptotic cells take 50 min to 1 h from the onset of phosphatidylserine externalization to plasma membrane rupture (Fig. 3*B*).

To trigger pyroptosis, LPS was transfected into the cytosol to activate caspase-11 (35). Unlike necroptosis and apoptosis, cells undergoing pyroptosis do not show overt signs of impending membrane rupture in the hours leading up to cell death, although

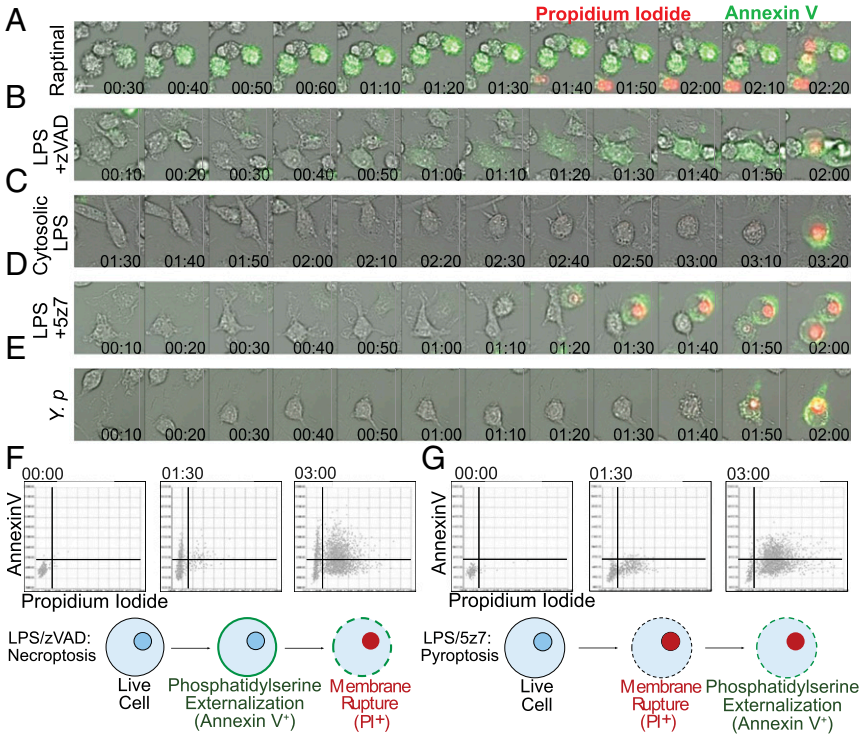

Fig. 3. *Yersinia*- and LPS/5z7-driven cell death resembles pyroptosis by morphology. (*A–E*) B6 BMDMs were stimulated as indicated. *Y.p.*, *Y. pseudotuberculosis*, MOI 5. Shown are 10-min frames from time-lapse microscopy performed at 40× magnification of annexin V and PI dual staining during the progression of cell death. Twelve frames preceding membrane rupture are shown to depict the 2 h of cell-death progression leading to loss of membrane integrity. (Scale bar: 10 μm.) (*F* and *G*, *Upper*) Cells stained with wheat germ agglutinin, annexin V, and PI were imaged at 4× magnification at 2-min intervals, with 4,000 cells per field of view. Annexin V and PI signals were extracted from wheat germ agglutinin-labeled cells, converted into numerical values, and plotted on the *y* axis for annexin V and on the *x* axis for PI. Representative time points of 0, 1.5, and 3 h are shown. (*Lower*) Cartoons depict our simplified model of the progression of phosphatidylserine externalization and membrane rupture during necroptosis or LPS/5z7-driven cell death. All imaging experiments are representative of three or more experiments.

a weak PI signal from the nuclei can be observed. PI nuclear signal is simultaneous with annexin V positivity as the cell balloons out into a spherical morphology (Fig. 3*C*).

With LPS/5z7 costimulation, dying cells retain extensive lammelipodia up to 10–20 min before membrane rupture. At 10 min before loss of membrane integrity, the cell shrinks rapidly, followed by simultaneous onset of weak annexin V positivity, blebbing, and a weak PI signal seeping into the nucleus. Within 10 min of annexin V binding the cell bursts with one large, spherical balloon along with full nuclear PI signal (Fig. 3*D*). The identical progression of cell death is seen during *Yersinia*-induced cell death (Fig. 3*E*).

To quantify this phenotype on a population level, images were taken at 4× magnification with 3,000–4,000 cells captured per frame. Annexin V and PI signal intensity per cell were plotted on the *y* and *x* axes, respectively. Representative frames at 1.5 and 3 h are shown for LPS/zVAD and LPS/5z7 (Fig. 3 *F* and *G* and Movies S1 and S2). On a population level, necroptotic cells show a distinct population of annexin V^+PI^- cells that transition into PI positivity (Fig. 3*F*). In contrast, LPS/5z7-stimulated cells progress from dual negative to a PI^+annexin V^{weak} state and gain annexin V positivity over time (Fig. 3*G*). Our data show that with TAK1 inhibition-induced cell death, the rapidity of membrane rupture curtails the process of phosphatidylserine externalization, leading to a pyroptotic-like cell-death morphology.

To support our morphological analysis, we performed TUNEL staining to detect DNA breaks indicative of the late stages of apoptosis. Within 220 min, 5% $TUNEL^+$ nuclei were detected in BMDMs treated with raptinal to induce apoptosis but were absent after treatment in necroptotic (LPS/zVAD) and pyroptotic (cytosolic LPS and LPS + ATP) conditions as well as after treatment with LPS/5z7 (*SI Appendix*, Fig. S3*A*).

Caspase-8 Induces GSDMD Cleavage to Drive Pyroptosis, Curtailing Apoptosis. GSDMD and gasdermin E (GSDME) are two effectors of pyroptosis downstream of caspase activation (12, 36). To determine whether GSDMD and GSDME are involved in LPS/5z7- and *Yersinia*-induced cell death, macrophages were stimulated with various cell-death stimulants, and cell lysates were probed for active cleavage products of GSDMD and GSDME. We observed that GSDMD and GSDME are both cleaved to generate the active p30 fragment within 3 h of LPS/5z7 stimulation as well as after *Yersinia* challenge (Fig. 4*A*). In addition to the active p30 fragment generated by caspase-1 and caspase-11 as previously described (12, 36), we also observe a higher GSDMD fragment (~40 kDa), likely the inactive p43 recently reported downstream of caspase-3 activity (37). Macrophages lacking GsdmD show a significant delay in PI incorporation during challenge with either LPS/5z7 or *Yersinia* (Fig. 4 *B* and *C*). Morphologically, the curtailed annexin V staining in GSDMD-sufficient cells became robust and prolonged with the loss of GSDMD, accompanied by an increase—albeit incremental—in $TUNEL^+$ nuclei, recapitulating an apoptotic morphology (Fig. 4 *D* and *E* and *SI Appendix*, Fig. S4*A*). This can be seen on a population view with LPS/5z7 that drives a synchronized cell-death response (Fig. 4*D*) as well as on an individual cellular basis during *Yersinia* infection (Fig. 4*E*). Loss of GSDME either singly or in conjunction with GSDMD loss did not confer further protection against LPS/5z7-induced death (*SI Appendix*, Fig. S4 *B* and *C*).

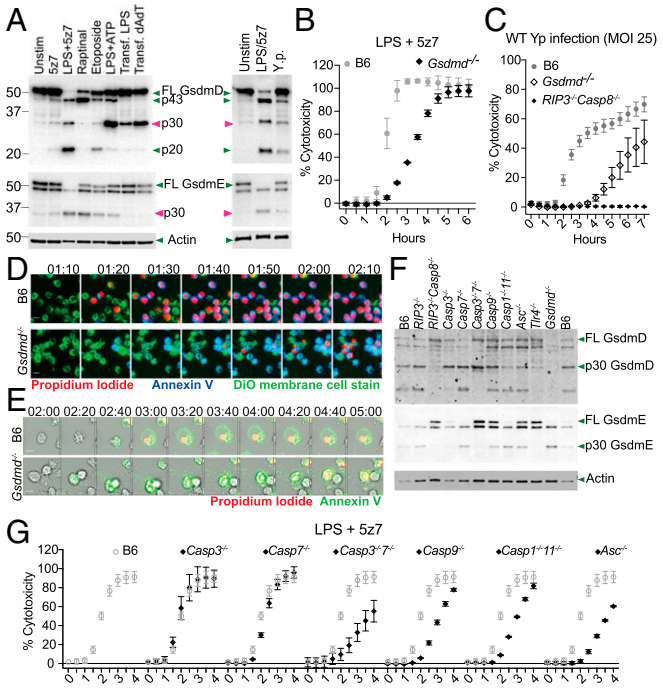

Fig. 4. Caspase-8 induces GsdmD cleavage to drive pyroptosis, curtailing apoptosis. (*A*) Cleavage products of GsdmD and GsdmE in cell lysate when BMDMs are stimulated with various cell-death triggers or *Yersinia* infection. The time point shown is 3 h post stimulation or infection with *Y. pseudotuberculosis* at an MOI of 25. (*B*) Cell-death kinetics by PI incorporation in B6 and *Gsdmd*$^{-/-}$ BMDMs stimulated with LPS/5z7. (*C*) Cell-death kinetics by PI incorporation in B6, *Gsdmd*$^{-/-}$, and *Rip3*$^{-/-}$*Casp8*$^{-/-}$ BMDMs infected with *Yersinia* (MOI 25). (*D*) Time-lapse microscopy of B6 and *GsdmD*$^{-/-}$ BMDMs triple stained with Neuro-DiO, annexin V, and PI imaged at 20× magnification. Cells were stimulated with LPS/5z7. Image series depict the hour leading up to membrane rupture in *GsdmD*$^{-/-}$ BMDMs. (Scale bars: 10 μm.) (*E*) Time-lapse microscopy of B6 and *GsdmD*$^{-/-}$ BMDMs triple stained with annexin V and PI imaged at 40× magnification. Cells were infected with *Yersinia* (MOI 5). Imaged series depict the 3 h leading to membrane rupture in *GsdmD*$^{-/-}$ BMDMs. (Scale bars: 10 μm.) (*F*) Cleavage products of GsdmD and GsdmE in cell lysate of BMDMs from various knockouts when stimulated with LPS/5z7 for 2 h. (*G*) LPS/5z7-driven cell-death kinetics by PI incorporation in BMDMs deficient for various caspases or ASC. The cytotoxicity curve of each genotype is superimposed over B6 cytotoxicity curves for clarity of comparison. All kinetic cytotoxicity data, Western blots, and imaging experiments are representative of three or more experiments.

To identify caspases responsible for the cleavage of GSDMD and GSDME, we stimulated macrophages from mice with various combinations of caspase knockouts with LPS/5z7 to observe gasdermin cleavage as well as cell death. We found that all three GSDMD cleavage products were abolished in *Rip3*$^{-/-}$ *Casp8*$^{-/-}$ macrophages (Fig. 4*F*). The p43 subunit is no longer present in *Casp3*$^{-/-}$ and *Casp3*$^{-/-}$*7*$^{-/-}$ macrophages with heightened presence of the p30 fragment. All three fragments are present in the *Casp9*$^{-/-}$ macrophages. *Casp1*$^{-/-}$*11*$^{-/-}$ and *Asc*$^{-/-}$ macrophages show a minor or no decrease in the appearance of p30 (Fig. 4*F*). The complete loss of all three fragments in the *Rip3*$^{-/-}$ *Casp8*$^{-/-}$ macrophages in conjunction with the minor loss of the p30 fragment in *Casp1*$^{-/-}$*11*$^{-/-}$ and *Asc*$^{-/-}$ macrophages shows that caspase-8 is necessary for the generation of active GSDMD during TAK1 inhibition.

In GSDME cleavage, as in GSDMD cleavage, the p30 fragment is absent in *Rip3*$^{-/-}$ *Casp8*$^{-/-}$ macrophages. The p30 fragment is mostly abolished in *Casp3*$^{-/-}$ macrophages and is completely abolished in *Casp3*$^{-/-}$*7*$^{-/-}$ macrophages (Fig. 4*F*). Therefore caspase-8 drives GSDME cleavage primarily via caspase-3 with minor a contribution from caspase-7, in agreement with published work (37).

Testing the caspase-knockout macrophages for cell death, we observed mild kinetic delays in *Casp3*$^{-/-}$*7*$^{-/-}$, *Casp9*$^{-/-}$, *Casp1*$^{-/-}$*11*$^{-/-}$, and *Asc*$^{-/-}$ macrophages (Fig. 4*G*). These delays in cell death are consistent with the model of overlapping functions of multiple effector proteins in driving cell death. Caspase-8 is the critical initiator that drives both arms of gasdermin activation, generating p30 fragments of GSDMD and GSDME. *Casp9*$^{-/-}$ shows no defect in the cleavage of either gasdermin but does display a mild delay in cell-death kinetics. Caspase-9 may drive mitochondrial dysfunction and reactive oxygen species accumulation, which has been previously reported during TAK1 inhibition (9, 38).

IL-1 Secretion Requires Two Distinct Cell Populations to Generate Signal 1 and Signal 2. NLRP3 activation via potassium efflux as a consequence of membrane pore formation has recently been shown to occur during both pyroptosis and necroptosis (22, 36). Potassium efflux-induced inflammasome activation thus may be a commonality shared among various necrotic modes of cell death (39). We therefore wanted to know if TAK1 inhibition-induced cell death, with its resemblance to pyroptosis in morphology, has the ability to induce inflammasome activation and IL-1 release.

Stimulation of BMDMs simultaneously with LPS/5z7 or with LPS alone did not lead to the release of IL-1 in the supernatant (Fig. 5*A*), perhaps unsurprisingly because of the requirement of MAPK and NFκB signaling for pro–IL-1 synthesis, which would be inhibited with 5z7. Much like IL-1, TNF is undetectable when TAK1 is inhibited by 5z7 (Fig. 5*B*). Using *Rip3*$^{-/-}$ *Casp8*$^{-/-}$ macrophages to bypass cell death, we found that 5z7 is still effective in blocking all pro–IL-1β induced by LPS stimulation (Fig. 5*C*). Similarly, at a *Y. pseudotuberculosis* multiplicity of infection (MOI) that is effective in inducing RIP3/caspase-8–dependent cell death (MOI 15), we find that pro–IL-1β synthesis is sufficiently blocked in the presence of YopJ (Fig. 5*D*).

Interestingly, and unlike agonist-driven cell death, during low-MOI *Yersinia* infection IL-1β and IL-1β are found in the supernatant in a RIP3/caspase-8–dependent manner (Fig. 5*E*). We observed an inverse correlation between IL-1β abundance and MOI, with lower *Yersinia* MOI correlating with higher cytokine levels in the supernatant (Fig. 5*E*). Of note, at the doses at which abundant IL-1β secretion is observed, cell death as measured by PI^{+} nuclei approaches the lower limit of detection (Fig. 5*F*). Peterson et al. have shown with TNF that during *Yersinia* infection, because the bacterial population does not uniformly translocate adequate levels of YopJ to fully block TAK1 activity, insufficiently TAK1-inhibited cells retain the ability to synthesize cytokines (40). Similarly, we observe that cellular pro–IL-1β is synthesized when the macrophage population is challenged with diminishing doses of YopJ-sufficient *Yersinia* (Fig. 5*G*).

IL-1β maturation requires an additional inflammasome signal to activate caspase-1. Given that IL-1β release is both inversely related to cell death and requires cell death for its maturation, we hypothesized that two cellular populations are needed to generate the two signals required for IL-1β production during *Yersinia* infection. We propose that pro–IL-1β is synthesized in cells that still retain TAK1 function. This population could be experiencing TLR activity via contact with less virulent bacteria in the inoculum or with bacterial-shed outer membrane vesicles (41). The inflammasome signal is provided by the TAK1-inhibited cells that are unable to synthesize cytokines but are driven to necrotic cell death via caspase-8–induced GSDMD activation. Upon the death of TAK1-inhibited cells, the release of active inflammasome results in the cleavage and maturation of IL-1β in pro–IL-1β–sufficient cells. Our line of thinking is supported by reports that oligomerized ASC and the functional NLRP3 inflammasome can have extracellular activity (42). Alternatively, the dying population of macrophages may be exposing

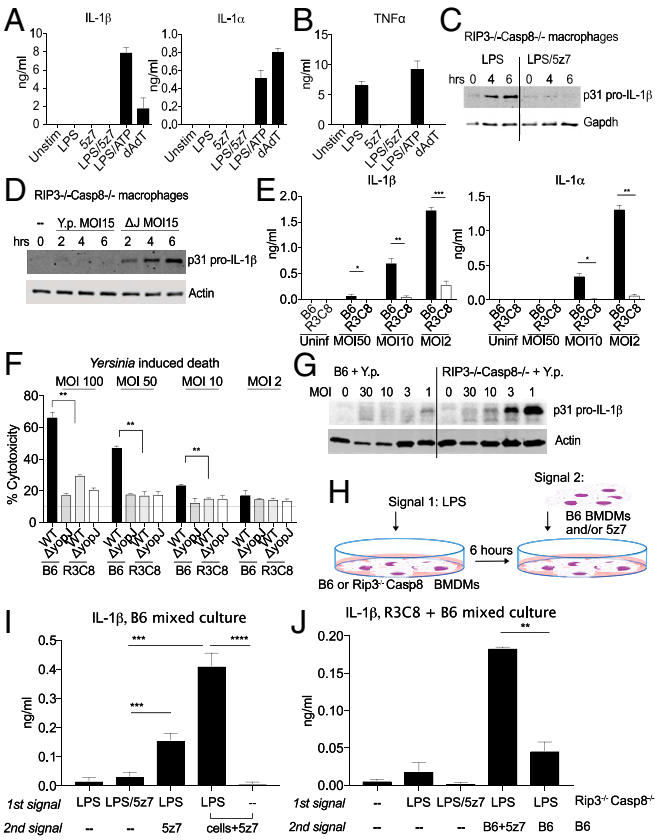

Fig. 5. IL-1 secretion requires two distinct cell populations to generate signal 1 and signal 2. (*A*) Supernatant IL-1α and IL-1β measured by ELISA 6 h post stimulation by LPS/5z7 compared with canonical inflammasome stimuli. (*B*) TNF secretion measured by ELISA 6 h post stimulation by LPS/5z7 compared with canonical inflammasome stimuli. (*C* and *D*) Pro–IL-1β from cell lysates of *Rip3*$^{-/-}$*Casp8*$^{-/-}$ BMDMs stimulated with agonists (*C*) or infected with *Yersinia* (MOI 15) (*D*) at the indicated time points. (*E*) Supernatant IL-1α andIL-1β measured by ELISA 16 h post *Yersinia* infection of B6 and *Rip3*$^{-/-}$*Casp8*$^{-/-}$ BMDMs as a function of decreasing bacterial MOI. (*F*) *Yersinia* YopJ-induced cytotoxicity in B6 and *Rip3*$^{-/-}$*Casp8*$^{-/-}$ BMDMs at 6 h post infection as a function of decreasing bacterial MOI. (*G*) YopJ-sufficient *Yersinia* infected at decreasing MOIs. Pro–IL-1β synthesis was measured from cell lysate of B6 and *Rip3*$^{-/-}$*Casp8*$^{-/-}$ BMDMs (16 h). (*H*) Experimental schematics for *I* and *J*. (*I*) IL-1β ELISA from B6 BMDMs asynchronously stimulated with the indicated signals with a 1-h interval between the first and second stimulus. The last two conditions represent the addition of B6 BMDMs and 5z7 for the second signal. (*J*) IL-1β ELISA from mixed cultures of B6 and *Rip3*$^{-/-}$*Casp8*$^{-/-}$ BMDMs asynchronously stimulated with the indicated signals with 1 h between the first and second stimulus. The first population of cells consists of *Rip3*$^{-/-}$*Casp8*$^{-/-}$ BMDMs plated overnight and experiencing the first signal for 1 h before the addition of the second signal. The second signal is either absent or is present in B6 BMDMs with or without 5z7. Time-point cytotoxicity quantifications and ELISA data are shown as ± SD from three independent experiments compared using Student's two-tailed *t* test: ns, nonsignificant ($P > 0.05$); *$P < 0.05$; **$P < 0.01$; ***$P < 0.001$. All Western blot data are representative of three or more experiments.

endogenous oxidized phospholipids from 1-palmitoyl-2-arachidonyl-sn-glycero-3-phosphorylcholine (PAPC) (also known as "oxPAPC"), which has recently been shown to be a potent inducer of IL-1 production in both macrophages and dendritic cells (43).

We tested this model by artificially generating two populations during LPS/5z7 treatment (Fig. 5 *H*–*J*). LPS serves as signal 1 to generate pro–IL-1 synthesis. Six hours later, 5z7 is added to the cells alone or in combination with a second population of naive cells (Fig. 5*H*). We found that, unlike cells treated simultaneously with LPS and 5z7, cultures in which cells experienced sequential LPS treatment followed by TAK1 inhibition released IL-1β into the supernatant. This effect is even more pronounced when the second cell population was added simultaneously with 5z7 (Fig. 5*I*).

Taking this one step further, we used *Rip3*$^{-/-}$ *Casp8*$^{-/-}$ macrophages as the LPS-primed population. Six hours after LPS stimulation, B6 BMDMs were added in the presence or absence of 5z7. Significantly elevated supernatant IL-1β was detected in mixed cultures that contained LPS-activated *Rip3*$^{-/-}$*Casp8*$^{-/-}$ cells and B6 cells in the presence of 5z7. Mixed cultures containing LPS-activated *Rip3*$^{-/-}$*Casp8*$^{-/-}$ cells and B6 cells in the absence of 5z7 did not produce significantly more IL-1β than homogeneous *Rip3*$^{-/-}$ *Casp8*$^{-/-}$ cell cultures stimulated with LPS alone (Fig. 5*J*). Our findings indicate that both a population of actively pyroptotic cells and a population of non-TAK1 inhibited cells are needed for IL-1 release.

Human Macrophages Are Resistant to TAK1 Inhibition-Induced Cell Death with No Consequent Secretion of IL-1β. In mouse macrophage cultures, YopJ-dependent cell death is observable across a range of bacteria MOIs. At high MOI, YopJ-independent cell death predominates, likely due to bacterial overload. YopJ-specific cell death is apparent at MOIs lower than 60, is optimal at MOIs around 30, and at lower doses approaching background levels (Fig. 6*A*). Human cells, in contrast, do not display a YopJ-dependent cell-death process at any MOI tested. We challenged human peripheral blood mononuclear cell (PBMC)-derived macrophages (Fig. 6*B*), the monocyte-like cell line U937 (*SI Appendix*, Fig. S5*A*), and monocyte-derived macrophages (*SI Appendix*, Fig. S5*B*). In all cases, bacterial outgrowth-induced cytotoxicity is readily observed at an MOI of 120. However, we were unable to detect YopJ-dependent cytotoxicity when cells were challenged with wild-type *Y. pseudotuberculosis* or the *ΔyopJ* mutant at MOIs ranging from 120 down to 15 (Fig. 6*B* and *SI Appendix*, Fig. S5 *A* and *B*). Similarly, human cells were resistant to killing by LPS/5z7 (Fig. 6 *C* and *D*), as is consistent with previously published work (38). With the additional treatment of zVAD, human cells underwent rapid necroptosis with dual annexin V and PI positivity (Fig. 6 *C* and *D*). With respect to cytokine production, the presence of YopJ reduces pro–IL-1β synthesis by human PBMC-derived macrophages (Fig. 6*E*, *Left*). Similarly, 5z7 effectively blocked LPS-induced pro–IL-1β synthesis (Fig. 6*E*, *Right*) and TNF production from PBMC- and monocyte-derived macrophages (Fig. 6*G* and *SI Appendix*, Fig. S5*D*). IL-1β levels in the supernatants of *Yersinia*-infected human PBMC- and monocyte-derived macrophages exposed to *Yersinia* infection are at the level of LPS-induced IL-1 secretion (Fig. 6*G* and *SI Appendix*, Fig. S5*C*). Lower MOIs did not increase IL-1 release into the supernatant, as is consistent with the lack of cell death-related inflammasome activation. In contrast, TNFα production after challenge with YopJ-sufficient *Y. pseudotuberculosis* did increase with diminishing MOI (Fig. 6*G* and *SI Appendix*, Fig. S5*D*), consistent with the findings of Peterson et al. (40) that reduced YopJ efficacy allows break-through of NFκB activity.

We considered the possibility that human macrophages may be able to up-regulate prosurvival factors more quickly with LPS stimulation, which would allow the cells to survive simultaneous LPS + 5z7 treatment. Indeed, when human PBMC-derived macrophages were pretreated for 2 h with 5z7 and then were stimulated with LPS, we were able to detect cell death (Fig. 6*H* and *SI Appendix*, Fig. S5*E*) as well as caspase activation and GSDME cleavage (Fig. 6*I*). Of note, we were unable to detect the p30 fragment of GSDMD. However, even with 5z7 pretreatment, the percentage of cell death was only modest, suggesting that prosurvival factors may be able to bypass TAK1 inhibition in human cells.

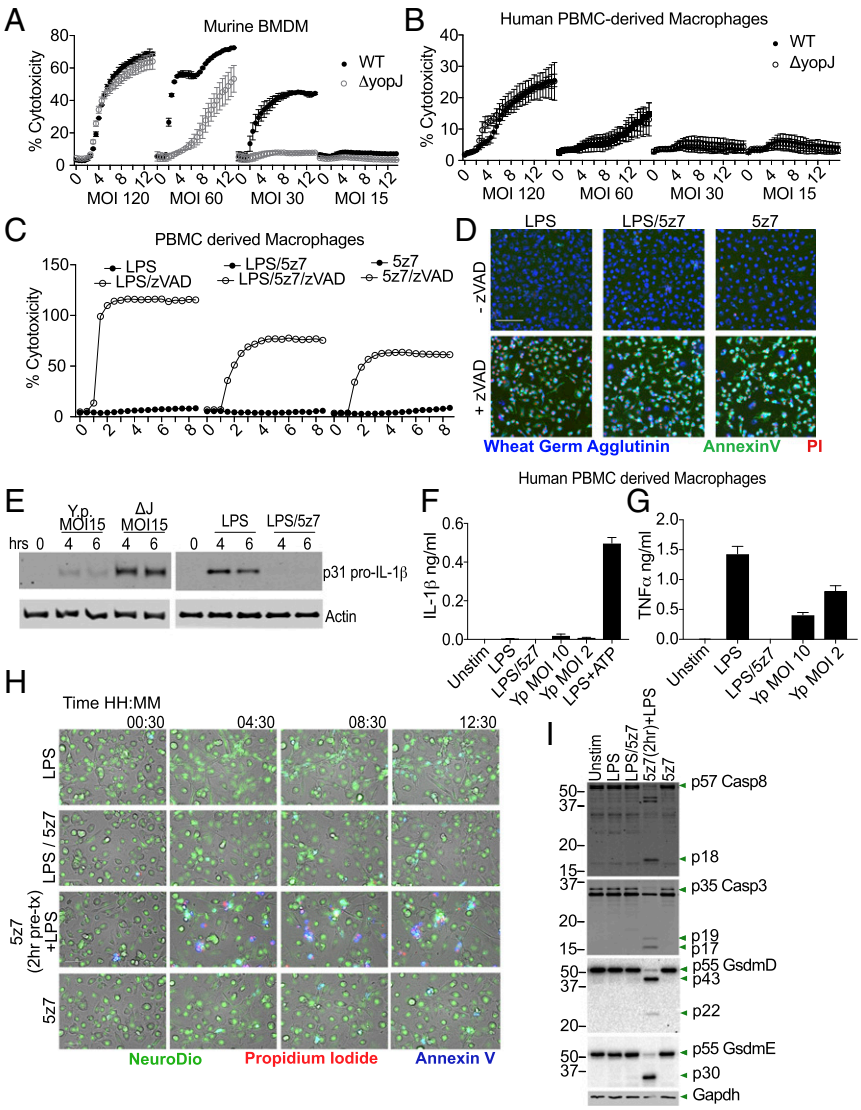

Fig. 6. Human macrophages are resistant to TAK1 inhibition-induced cell death with no consequent secretion of IL-1. (*A*) *Yersinia*-induced murine macrophage cell death at various bacterial MOIs; MOIs of 60–30 show YopJ-specific cell death. (*B*) *Yersinia*-induced death of human monocyte-derived macrophages. Bacteria were infected at multiple MOIs with no YopJ-dependent killing observed. (*C*) Human PBMC-derived macrophages were treated with LPS, LPS/5z7, or 5z7 in the presence or absence of zVAD (50 μM). Kinetics of cell death was measured by PI^+ nuclei. (*D*) Representative images of triple-stained human PBMC-derived macrophages taken at 4× magnification. PBMC-derived macrophages were stimulated as in *C*. The image shown is at 7.5 h post stimulation. (Scale bar: 100 m.) (*E*) Pro–IL-1β from cell lysates of human PBMC-derived macrophages challenged with *Yersinia* at the indicated MOI and time points (*Left*) or stimulated with LPS ± 5z7 (*Right*). (*F* and *G*) Supernatant IL-1β (*F*) and TNF (*G*) from human PBMC-derived macrophages stimulated with LPS/5z7 or *Yersinia* at MOIs that elicit robust IL-1α/β secretion from murine macrophages. (*H*) Human PBMC-derived macrophages were stimulated with the indicated conditions and kinetically imaged with triple staining (Neuro-DiO, PI, and annexin V). The second row from the bottom involved a 2-h 5z7 pretreatment before LPS stimulation. (*I*) Human PBMC-derived macrophages were stimulated with the indicated conditions for 4 h and were analyzed by Western blotting for caspase-8 and caspase-3 cleavage as well as GSDMD and GSDME. The second-to-last condition involved 2 h of 5z7 pretreatment before LPS stimulation. All kinetic cytotoxicity data, Western blots, ELISAs, and imaging experiments are representative of three or more experiments.

Discussion

In the present study, we demonstrate that *Yersinia* YopJ-induced murine macrophage death involved caspase-8–induced cleavage of both GSDMD and GSDME. The ensuing cell death is rapid, morphologically pyroptotic, and induces IL-1 release (Fig. 7). At the time of the writing this paper, work from the Kanneganti laboratory reported that the genetic ablation of TAK1 from myeloid cells resulted in spontaneous cell death during macrophage maturation (44). Their work shows that loss of TAK1 leads to spontaneous cell death, NLRP3 activation, and IL-1 production in macrophages due to tonic TNF signaling. The genetic ablation of TAK1 by the Kanneganti laboratory complements our work with *Yersinia* infection and acute TAK1 inhibition with 5z7, providing further evidence for the central role of TAK1 in cell death and inflammation.

GSDMD is a critical effector of pyroptosis which disrupts cell membranes upon cleavage by caspase-1/-11 (12, 36, 45). Similarly, GSDME is an effector driving necrosis downstream of caspase-3 (33, 46). These findings prompted the Shao group to redefined pyroptosis as cell death mediated by gasdermin activation (47). Our work extends these studies and shows that activation of caspase-8 in the context of TAK1 inhibition results in cleavage of GSDMD, leading to a pyroptotic-like cell death. Further study is needed to determine whether caspase-8 can cleave GSDMD directly or if other intermediary substrates independent of

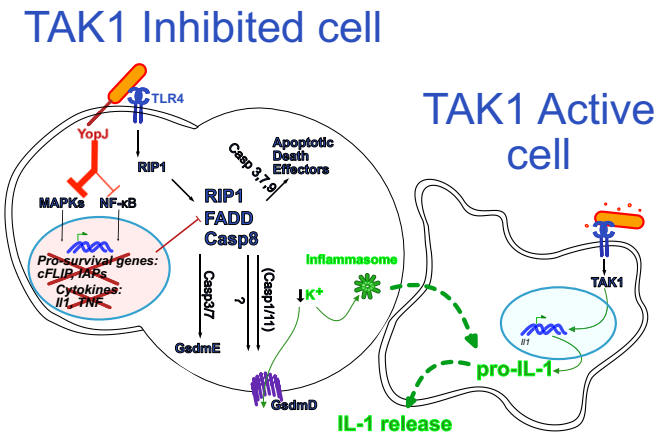

Fig. 7. Model of *Yersinia*-induced cell death and IL-1 production. Two mouse macrophages are illustrated. The macrophage on the left (a TAK1-inhibited dying cell) is sufficiently intoxicated with *Yersinia* YopJ to inhibit TAK1. The bacterium is also recognized by TLR4, which signals via RIP1 to form a cell-death complex composed of RIP1, caspase-8, and, likely, FADD. This death complex drives GsdmD cleavage and activation partially via caspase-1/11 and GsdmE cleavage via caspase-3 and caspase-7, both of which result in cell membrane permeabilization and subsequent cell death. There are likely additional effectors of cell death-driven activation, which in conjunction with GsdmD may lead to potassium flux out of the cell and subsequent inflammasome activation. A second macrophage that is not sufficiently intoxicated by YopJ is necessary for the production of pro–IL-1 cytokines. Upon contact with the dying cell or cellular components, IL-1 maturation occurs. See *Discussion* for details.

casppase-1/11 are required to generate the pore-forming p30 subunit. Additionally, the cell-death response is only kinetically delayed in *Gsdmd*$^{-/-}$ macrophages, suggesting that the activation of other cell-death effectors may be engaged to ensure the eventual demise of the cell under TAK1 inhibition.

Gasdermin cleavage may have functions beyond cellular obliteration. Work by both the Shao and Lieberman laboratories elegantly demonstrated that cleaved GSDMD can attack bacteria and reduce their viability (48). Other work by the Miao laboratory has shown that pyroptosis can result in pore-induced intracellular traps, leading to the retention of intracellular bacteria within the carcass of dying cells to facilitate phagocytic clearance (49). Jorgensen's work places the importance of macrophage pyroptosis into an in vivo context, in which IL-1 production during pyroptosis recruits secondary phagocytic cells to the site of infection to engulf dead cell carcasses along with its damaged bacterial load.

During traditionally pyroptotic infections such as with *Legionella*, *Salmonella*, *Francisella*, and *Burkholdia*, IL-1 maturation is intrinsic to the infected, dying cell (50). The case of *Yersinia* infection is particularly interesting, since MAPK signaling is inhibited by YopJ, effectively blocking pro–IL-1 synthesis in doomed, infected macrophages (30, 31). Since bacterial populations are not homogenous in their virulence, some percentage of macrophages at the site of infection will not be sufficiently intoxicated by YopJ, thus retaining the ability to synthesize MAPK-dependent cytokines. We postulate that these MAPK-competent cells are also the producers of pro–IL-1, with neighboring pyroptosing cells serving as platforms for potassium efflux-induced inflammasome formation (Fig. 7). We predict that the MAPK-competent cells then complete the processing of IL-1 maturation by efferocytosing dead cells or by acquiring extracellular ASC/NLRP3 inflammasomes released by dying cells. Alternatively, the live macrophages may be sensing endogenous oxidized lipids, such as oxPAPC from dying cells, which are known to induce IL-1 production in macrophages and dendritic cells via activation of caspase-11 (51).

Taken together, these findings indicate that macrophages that are defective for the cell-death response, such as *Rip3*$^{-/-}$ *Casp8*$^{-/-}$ and RIP1 kinase dead (RIP1^{K45A}), would therefore be defective in IL-1 maturation as well, making the animals more susceptible to uncontrolled *Yersinia* replication (15). Extending this line of argument, we found that human macrophages with minimal production of IL-1 during *Yersinia* infection do not undergo YopJ-dependent cell death, an observation that may provide some insight into the devastation caused by the plague. In the present study, we used IP2666 *Y. pseudotuberculosis*, which expresses hexaacylated LPS capable of triggering TLR4. The more dangerous *Y. pestis* evolved from *Y. pseudotuberculosis* and in the process acquired a hypoacylated TLR4-evasive LPS (52). Additionally, hypoacylated lipid IVa acts as an antagonist for TLR4 activation in human macrophages, although it is weakly stimulatory against TLR4 of murine macrophages (53). With YopJ inhibition of TAK1 tolerated by human macrophages, in combination with a TLR-4–evasive LPS structure, *Y. pestis* effectively creates a silent infection. This point has been elegantly demonstrated by the forced expression of *Escherichia coli* LPS on the Kim4 strain of *Y. pestis* as an attenuation strategy (54).

Other examples of necrotic forms of cell death lending protection to the infected host can be found in studies of necroptosis. For instance, RIP3 has been shown to be protective in the case of vaccinia virus infection and CMV infection (55) and during HSV replication by the induction of cell death in infected mouse cells (56). In the case of HSV, necroptosis in mouse cells limits viral replication, while the absence of necroptosis in human cells leads to uncontrolled viral replication. These findings with HSV bear striking similarity to the differential species-based cell-death responses and pathogen replication highlighted in our study.

Human macrophages therefore may have an inborn tolerance to highly pathogenic bacterial neighbors, to the detriment of the organism. At the macrophage level, the resistance to cell death may lie in the higher expression or longer half-life of key prosurvival proteins. In mouse macrophages, complex IIa forms when there are inadequate prosurvival factors, including cellular FLICE-inhibitory protein (cFLIP) (57) and inhibitors of apoptosis (IAPs) (25). More recent work has also implicated the loss of IAP and cFLIP during TAK1 inhibition as a reason for cell death (58). IAPs and FLIP are top candidates in the investigation of how the regulation of these proteins results in in a cell-death defect in human macrophages.

Very recent investigations in the field of cell death also show that MAPK-activated protein kinase 2, a downstream target of P38 and TAK1, is required for RIP1 phosphorylation at Ser321 (59). This MAPK-driven RIP1 phosphorylation inhibits complex II formation and thus limits cell death. The state of RIP1 regulation in human macrophages may also be an area of interest.

The differential response of human and murine macrophages demonstrated by our study and others (56) thus calls attention to the need to study both mouse and human cells to understand the course of illness in humans, especially when rodents are reservoirs for the human disease of interest. Beyond *Yersinia*, the anthrax toxin and lethal factor effectors of *Bacillus anthracis* inhibit MAPK activation and have been observed to elicit cell death and IL-1 production (60). Investigating the role of gasdermins and the presence of pyroptotic features in this and other infectious systems known to inhibit MAPK or NFκB signaling may provide a deeper understanding of the mechanism and scope of necrotic cell death in host defense.

Materials and Methods

Wild-type and ΔyopJ IP2666 *Y. pseudotuberculosis* strains were gifts from Ralph Isberg, Tufts University School of Medicine, Boston, and Joan Mecsas, Tufts University School of Medicine, Boston, and were grown on LB plates containing Irgasan (Sigma-Aldrich). Overnight cultures grown at 26 °C were

diluted to an OD_{600} of 0.2 and were grown at 26 °C for 2 h followed by 37 °C for 2 h. Macrophage cultures were infected at the MOI ranges indicated in the figures and their legends. Macrophages were harvested from mice housed in a pathogen-free facility at the Tufts University School of Medicine, and experiments were performed in accordance with regulations and approval of the Tufts University Institutional Animal Care and Use Committee. Statistical analysis was performed using the Student's *t* test (two-tailed) using GraphPad Prism; $*P < 0.05$; $**P < 0.01$; $***P < 0.001$. Detailed methods are provided in *SI Appendix, SI Materials and Methods*.

ACKNOWLEDGMENTS. We thank Dr. Ralph Isberg and Dr. Joan Mecsas for the gift of *Y. pseudotuberculosis*. We thank Dr. Kate Fitzgerald and Dr. Egil Lien for insightful discussions and sharing of bones from various genetic knockout animals, and Dr. Yinan Gong and Dr. Brigitte Huber for suggestions and guidance at various phases of this project. This work was supported by National Institute of Allergy and Infectious Disease (NIAID) Grant AI135369 and Russian Science Fund Project 15-15-00100 (to A.P.) and NIAID Grant T32-AI-007077 to the Immunology Graduate Program (Tufts University).

1. O'Neill LA, Golenbock D, Bowie AG (2013) The history of toll-like receptors–Redefining innate immunity. *Nat Rev Immunol* 13:453–460.
2. Reddick LE, Alto NM (2014) Bacteria fighting back: How pathogens target and subvert the host innate immune system. *Mol Cell* 54:321–328.
3. Park JM, et al. (2005) Signaling pathways and genes that inhibit pathogen-induced macrophage apoptosis–CREB and NF-kappaB as key regulators. *Immunity* 23:319–329.
4. Chen G, Goeddel DV (2002) TNF-R1 signaling: A beautiful pathway. *Science* 296: 1634–1635.
5. Kelliher MA, et al. (1998) The death domain kinase RIP mediates the TNF-induced NF-kappaB signal. *Immunity* 8:297–303.
6. Micheau O, Tschopp J (2003) Induction of TNF receptor I-mediated apoptosis via two sequential signaling complexes. *Cell* 114:181–190.
7. Murphy JM, et al. (2013) The pseudokinase MLKL mediates necroptosis via a molecular switch mechanism. *Immunity* 39:443–453.
8. Kaiser WJ, et al. (2013) Toll-like receptor 3-mediated necrosis via TRIF, RIP3, and MLKL. *J Biol Chem* 288:31268–31279.
9. Omori E, Morioka S, Matsumoto K, Ninomiya-Tsuji J (2008) TAK1 regulates reactive oxygen species and cell death in keratinocytes, which is essential for skin integrity. *J Biol Chem* 283:26161–26168.
10. Sato S, et al. (2005) Essential function for the kinase TAK1 in innate and adaptive immune responses. *Nat Immunol* 6:1087–1095.
11. Bergsbaken T, Fink SL, Cookson BT (2009) Pyroptosis: Host cell death and inflammation. *Nat Rev Microbiol* 7:99–109.
12. Aglietti RA, et al. (2016) GsdmD p30 elicited by caspase-11 during pyroptosis forms pores in membranes. *Proc Natl Acad Sci USA* 113:7858–7863.
13. Rajput A, et al. (2011) RIG-I RNA helicase activation of IRF3 transcription factor is negatively regulated by caspase-8-mediated cleavage of the RIP1 protein. *Immunity* 34:340–351.
14. Viboud GI, Bliska JB (2005) Yersinia outer proteins: Role in modulation of host cell signaling responses and pathogenesis. *Annu Rev Microbiol* 59:69–89.
15. Paquette N, et al. (2012) Serine/threonine acetylation of TGFβ-activated kinase (TAK1) by Yersinia pestis YopJ inhibits innate immune signaling. *Proc Natl Acad Sci USA* 109: 12710–12715.
16. Monack DM, Mecsas J, Ghori N, Falkow S (1997) Yersinia signals macrophages to undergo apoptosis and YopJ is necessary for this cell death. *Proc Natl Acad Sci USA* 94: 10385–10390.
17. Philip NH, et al. (2014) Caspase-8 mediates caspase-1 processing and innate immune defense in response to bacterial blockade of NF-κB and MAPK signaling. *Proc Natl Acad Sci USA* 111:7385–7390.
18. Peterson LW, et al. (2017) RIPK1-dependent apoptosis bypasses pathogen blockade of innate signaling to promote immune defense. *J Exp Med* 214:3171–3182.
19. Ratner D, et al. (2016) Manipulation of interleukin-1β and interleukin-18 production by Yersinia pestis effectors YopJ and YopM and redundant impact on virulence. *J Biol Chem* 291:16417.
20. Lawlor KE, et al. (2015) RIPK3 promotes cell death and NLRP3 inflammasome activation in the absence of MLKL. *Nat Commun* 6:6282.
21. He WT, et al. (2015) Gasdermin D is an executor of pyroptosis and required for interleukin-1β secretion. *Cell Res* 25:1285–1298.
22. Conos SA, et al. (2017) Active MLKL triggers the NLRP3 inflammasome in a cell-intrinsic manner. *Proc Natl Acad Sci USA* 114:E961–E969.
23. Wu J, et al. (2013) Mechanism and in vitro pharmacology of TAK1 inhibition by (5Z)-7-oxozeaenol. *ACS Chem Biol* 8:643–650.
24. Degterev A, et al. (2008) Identification of RIP1 kinase as a specific cellular target of necrostatins. *Nat Chem Biol* 4:313–321.
25. Tenev T, et al. (2011) The ripoptosome, a signaling platform that assembles in response to genotoxic stress and loss of IAPs. *Mol Cell* 43:432–448.
26. Giroir BP, Brown T, Beutler B (1992) Constitutive synthesis of tumor necrosis factor in the thymus. *Proc Natl Acad Sci USA* 89:4864–4868.
27. Gough DJ, Messina NL, Clarke CJ, Johnstone RW, Levy DE (2012) Constitutive type I interferon modulates homeostatic balance through tonic signaling. *Immunity* 36: 166–174.
28. Taylor RC, Cullen SP, Martin SJ (2008) Apoptosis: Controlled demolition at the cellular level. *Nat Rev Mol Cell Biol* 9:231–241.
29. Hande KR (1998) Etoposide: Four decades of development of a topoisomerase II inhibitor. *Eur J Cancer* 34:1514–1521.
30. Palmer LE, Pancetti AR, Greenberg S, Bliska JB (1999) YopJ of Yersinia spp. is sufficient to cause downregulation of multiple mitogen-activated protein kinases in eukaryotic cells. *Infect Immun* 67:708–716.
31. Rosadini CV, et al. (2015) A single bacterial immune evasion strategy dismantles both MyD88 and TRIF signaling pathways downstream of TLR4. *Cell Host Microbe* 18: 682–693.
32. Palchaudhuri R, et al. (2015) A small molecule that induces intrinsic pathway apoptosis with unparalleled speed. *Cell Rep* 13:2027–2036.
33. Rogers C, et al. (2017) Cleavage of DFNA5 by caspase-3 during apoptosis mediates progression to secondary necrotic/pyroptotic cell death. *Nat Commun* 8:14128.
34. Gong YN, et al. (2017) ESCRT-III acts downstream of MLKL to regulate necroptotic cell death and its consequences. *Cell* 169:286–300.e16.
35. Kayagaki N, et al. (2013) Noncanonical inflammasome activation by intracellular LPS independent of TLR4. *Science* 341:1246–1249.
36. Kayagaki N, et al. (2015) Caspase-11 cleaves gasdermin D for non-canonical inflammasome signalling. *Nature* 526:666–671.
37. Taabazuing CY, Okondo MC, Bachovchin DA (2017) Pyroptosis and apoptosis pathways engage in bidirectional crosstalk in monocytes and macrophages. *Cell Chem Biol* 24:507–514.e4.
38. Wang JS, Wu D, Huang DY, Lin WW (2015) TAK1 inhibition-induced RIP1-dependent apoptosis in murine macrophages relies on constitutive TNF-α signaling and ROS production. *J Biomed Sci* 22:76.
39. Wallach D, Kang TB, Dillon CP, Green DR (2016) Programmed necrosis in inflammation: Toward identification of the effector molecules. *Science* 352:aaf2154.
40. Peterson LW, et al. (2016) Cell-extrinsic TNF collaborates with TRIF signaling to promote Yersinia-induced apoptosis. *J Immunol* 197:4110–4117.
41. Jung AL, et al. (2017) Legionella pneumophila infection activates bystander cells differentially by bacterial and host cell vesicles. *Sci Rep* 7:6301.
42. Franklin BS, et al. (2014) The adaptor ASC has extracellular and 'prionoid' activities that propagate inflammation. *Nat Immunol* 15:727–737.
43. Zanoni I, et al. (2016) An endogenous caspase-11 ligand elicits interleukin-1 release from living dendritic cells. *Science* 352:1232–1236.
44. Malireddi RKS, et al. (2018) TAK1 restricts spontaneous NLRP3 activation and cell death to control myeloid proliferation. *J Exp Med* 215:1023–1034.
45. Gaidt MM, Hornung V (2016) Pore formation by GSDMD is the effector mechanism of pyroptosis. *EMBO J* 35:2167–2169.
46. Wang Y, et al. (2017) Chemotherapy drugs induce pyroptosis through caspase-3 cleavage of a gasdermin. *Nature* 547:99–103.
47. Shi J, Gao W, Shao F (2017) Pyroptosis: Gasdermin-mediated programmed necrotic cell death. *Trends Biochem Sci* 42:245–254.
48. Liu X, et al. (2016) Inflammasome-activated gasdermin D causes pyroptosis by forming membrane pores. *Nature* 535:153–158.
49. Jorgensen I, Zhang Y, Krantz BA, Miao EA (2016) Pyroptosis triggers pore-induced intracellular traps (PITs) that capture bacteria and lead to their clearance by efferocytosis. *J Exp Med* 213:2113–2128.
50. Meunier E, et al. (2015) Guanylate-binding proteins promote activation of the AIM2 inflammasome during infection with Francisella novicida. *Nat Immunol* 16: 476–484.
51. Zanoni I, Tan Y, Di Gioia M, Springstead JR, Kagan JC (2017) By capturing inflammatory lipids released from dying cells, the receptor CD14 induces inflammasome-dependent phagocyte hyperactivation. *Immunity* 47:697–709.e3.
52. Chain PS, et al. (2004) Insights into the evolution of Yersinia pestis through whole-genome comparison with Yersinia pseudotuberculosis. *Proc Natl Acad Sci USA* 101: 13826–13831.
53. Golenbock DT, Hampton RY, Qureshi N, Takayama K, Raetz CR (1991) Lipid A-like molecules that antagonize the effects of endotoxins on human monocytes. *J Biol Chem* 266:19490–19498.
54. Montminy SW, et al. (2006) Virulence factors of Yersinia pestis are overcome by a strong lipopolysaccharide response. *Nat Immunol* 7:1066–1073.
55. Upton JW, Kaiser WJ, Mocarski ES (2012) DAI/ZBP1/DLM-1 complexes with RIP3 to mediate virus-induced programmed necrosis that is targeted by murine cytomegalovirus vIRA. *Cell Host Microbe* 11:290–297.
56. Huang Z, et al. (2015) RIP1/RIP3 binding to HSV-1 ICP6 initiates necroptosis to restrict virus propagation in mice. *Cell Host Microbe* 17:229–242.
57. Ram DR, et al. (2016) Balance between short and long isoforms of cFLIP regulates Fas-mediated apoptosis in vivo. *Proc Natl Acad Sci USA* 113:1606–1611.
58. Guo X, et al. (2016) TAK1 regulates caspase 8 activation and necroptotic signaling via multiple cell death checkpoints. *Cell Death Dis* 7:e2381.
59. Geng J, et al. (2017) Regulation of RIPK1 activation by TAK1-mediated phosphorylation dictates apoptosis and necroptosis. *Nat Commun* 8:359.
60. Park JM, Greten FR, Li ZW, Karin M (2002) Macrophage apoptosis by anthrax lethal factor through p38 MAP kinase inhibition. *Science* 297:2048–2051.